



Electrochemical investigation of the influence of thin SiO_x films deposited on gold on charge transfer characteristics

Sabine Szunerits^{a,c,*}, Carolina Nunes Kirchner^b, Gunther Wittstock^b,
Rabah Boukherroub^c, Chantal Gondran^d

^a Laboratoire d'Electrochimie et de Physicochimie des Matériaux et des Interfaces (LEPMI), CNRS-INPG-UJF, 1130 rue de la piscine, BP 75, 38402 St. Martin d'Hères Cedex, France

^b Carl von Ossietzky University Oldenburg, Faculty of Mathematics and Natural Sciences, Center of Interface Science (CIS), Department of Pure and Applied Chemistry and Institute of Chemistry and Biology of the Marine Environment, D-26111 Oldenburg, Germany

^c Institut de Recherche Interdisciplinaire (IRI), USR CNRS-3078, Institut d'Electronique, de Microélectronique et de Nanotechnologie (IEMN), UMR CNRS-8520, Cité Scientifique, Avenue Poincaré, BP 60069, 59652 Villeneuve d'Ascq, France

^d Département de Chimie moléculaire (UMR-CNRS-5250), Institut de Chimie Moléculaire de Grenoble (FR-CNRS 2607), Université Joseph Fourier, BP 53, F-38041 Grenoble Cedex 9, France

ARTICLE INFO

Article history:

Received 8 February 2008

Received in revised form 15 May 2008

Accepted 18 May 2008

Available online 6 June 2008

Keywords:

Silicon dioxide

Gold–silicon composite films

Plasma-enhanced chemical vapor deposition (PECVD)

Impedance

Scanning electrochemical microscopy (SECM)

ABSTRACT

The paper reports on the investigation of the electrochemical behavior of a thin gold film electrode coated with silicon dioxide (SiO_x) layers of increasing thickness. Stable thin films of amorphous silica (SiO_x) were deposited on glass slides coated with a 5 nm adhesion layer of titanium and 50 nm of gold, using plasma-enhanced chemical vapor deposition (PECVD) technique. Scanning electrochemical microscopy (SECM) and electrochemical impedance spectroscopy (EIS) were used to investigate the electrochemical behavior of the interfaces. In the case of SECM, the influence of the SiO_x thicknesses on the electron transfer kinetics of three redox mediators was investigated. Normalized current–distance curves (approach curves) were fitted to the theoretical model in order to find the effective heterogeneous first order rate constant (k_{eff}) at the sample. EIS was in addition used to confirm the diffusion barrier character of the SiO_x interlayer.

© 2008 Elsevier Ltd. All rights reserved.

1. Introduction

Self-assembled monolayers and Langmuir–Blodgett films deposited on metals and semiconductors have been extensively used and studied due to their fundamental importance in fine-tuning the bulk material properties. They enable to cause drastic and controlled changes to the wetting, adhesion, corrosion and electron transfer properties and have many applications in several areas of science and technology. Next to these organic materials, silica-based materials have attracted considerable attention as effective barrier layers as well as for chemical and biological sensing due to the high reactivity of their surface silanol groups enabling the immobilization of different molecules through silane coupling chemistry [1–6]. Controlled thin SiO₂ films on Si are mainly produced through plasma-activated chemical vapor deposition approaches. SiO₂ is an important insulating material in the

fabrication of semiconductor devices [7] and is used as an inter-metal dielectric material and transistor gate dielectric layer [8]. The formation of silica films on gold could be achieved by thermal evaporation of silicon dioxide in the presence of oxygen at low pressure [9], using a multitarget magnetron sputtering system [10], or low temperature sol–gel chemistry [1,2,5,9,11–14]. Due to the instability of the SiO₂/gold interfaces upon immersion in water [9], an adhesion layer of 2 nm titanium between gold and the silicon dioxide film was often added [15–18]. We have recently shown that thin layers of SiO_x deposited on gold films (with no intervening adhesion layer) by enhanced chemical vapor deposition (PECVD) are chemically and mechanically stable under various conditions [19–21]. In addition these interfaces were adaptable for surface plasmon resonance (SPR) detection [19–21] and PM-IRRAS investigations [22,23]. While SPR signals could be detected for SiO_x thicknesses ranging from 7 to 40 nm, the use of these interfaces for electrochemical detection schemes depends, however, strongly on the thickness of the oxide film. Cyclic voltammetry could be only performed on films thinner than 9 nm. Electrochemical impedance spectroscopy has shown to be highly useful to understand the

* Corresponding author. Tel.: +33 4 76 82 65 52.

E-mail address: sabine.szunerits@lepmi.inpg.fr (S. Szunerits).

packing density and distribution of pinhole defects in monolayers. The technique shows that the dynamics of charge transfer at the electrochemical interface is strongly influenced by the nature of the electrode surface and the structure of the electrical double layer. Scanning electrochemical microscopy (SECM) is an additional powerful technique for investigation of mass transport as it combines high-resolution visualization of surface topography with interfacial chemical and electrochemical reactivity information [24]. It is thus adapted to investigate the molecular transport of different electrochemical mediators through the nanostructured or porous layers [25,26]. The kinetics of the heterogeneous electron transfer (ET) of semiconductors have been studied using SECM approach curves in the feedback mode [27–29] and showed that ET rate can be controlled by applying different overpotentials ($E_s - E^{o'}$) to the sample. Pust et al. [28,29] and Neufeld et al. [30] showed that the ET kinetics at the solid/liquid interfaces change strongly depending on the redox potential of the mediator with respect to the energetic position of the bandgap of the semiconductor. An advantage in using SECM to analyze the kinetics of ET at the sample is that errors due to ohmic resistance and charging current are negligible.

In this paper we investigate in more details the effect of silicon oxide layer thickness deposited on gold on the electron transfer using electrochemical impedance spectroscopy. In fact most EIS studies have been performed on a Si/SiO₂ interface where space charge layer of the semiconductor will influence the electrochemical response. Here only the Helmholtz double layer capacitance on the gold interface will have to be taken into account. We show that by performing EIS measurements at high frequencies information about the insulating SiO₂ layer can be obtained. Furthermore we have used the feedback mode of SECM to record the approach curves to SiO_x layers different thicknesses to extract the effective heterogeneous first order rate constants (k_{eff}).

2. Experimental

2.1. Materials

Potassium chloride (KCl), potassium hexacyanoferrate-II ([Fe(CN)₆]⁴⁻), potassium hexacyanoferrate-III ([Fe(CN)₆]³⁻), potassium hexachloroiridate (K₃[IrCl₆]), ruthenium hexamine chloride ([Ru(NH₃)₆]Cl₃) and ferrocene methanol (FcMeOH) were obtained from Aldrich and used without further purification.

2.2. Preparation of the gold/SiO₂ composite slides

Substrate electrodes were prepared by thermal evaporation of 5 nm of titanium and 50 nm of gold onto cleaned glass slides (76 mm × 26 mm × 1 mm, $n = 1.58$ at $\lambda = 633$ nm CML, France). Prior to silica film deposition, the gold samples were first degreased in isopropanol and acetone in an ultrasound bath at room temperature, rinsed copiously with Milli-Q water and dried under a stream of nitrogen. The gold slides were then heated in the plasma chamber to 300 °C at a pressure of 0.005 Torr for 1 h. SiO_x layers were synthesized by plasma enhanced chemical vapor deposition in a Plasmalab 800Plus (Oxford Instruments, UK). The growth conditions used were as follows: substrate temperature: 300 °C; gas mixture: SiH₄ (3% in N₂) and N₂O (the gas flow was 260 sccm and 700 sccm for SiH₄ and N₂O, respectively); total pressure in the reactor: 1 Torr; power: 10 W at 13.56 MHz. Under these experimental conditions, the deposition rate was 41.4 nm min⁻¹ and the silica films display a refractive index of 1.48. We have adjusted the silica films thicknesses by varying the deposition time.

2.3. Instrumentation

2.3.1. Electrochemical instrumentation

Electrochemical impedance spectroscopy (EIS) and cyclic voltammetry experiments were performed using an Autolab potentiostat 100 (Eco Chemie, Utrecht, The Netherlands). EIS was performed with the following parameters: amplitude of 10 mV at open circuit potential with a frequency range of 10 kHz to 1 Hz. The electrolyte was KCl (0.1 M)/water. The electrochemical cell is the double-channel cell of the Autolab ESPRIT Instrument (Eco Chemie, Utrecht, The Netherlands) allowing simultaneous surface plasmon resonance and electrochemical measurements to be performed. The configuration of this equipment is described elsewhere [31,32]. The instrument is equipped with an electrochemical open cuvette system of 20–150 μ l sample volume where an Ag/AgCl reference electrode, a platinum counter electrode and a fixed contact point to the gold layer of the sensor chip are incorporated. The active electrode surface is 0.07 cm². The SPR part of the set up has not been used in this work. As these interfaces were used for coupled SPR and electrochemical impedance studies we preferred keeping the same set up.

2.3.2. SECM set up

A home-built SECM instrument was used to record the images. The SECM set up consists of a stepper motor positioning system (Märzhäuser Wetzlar GmbH & Co KG, Wetzlar, Germany), an ADC board (PCI-DAS 1602/16, Plug-in Electronic GmbH, Eichenau, Germany) and bipotentiostat (CHI 7001B, CH Instruments, Austin, TX, USA). The motor position and data acquisition are controlled by a homemade program written in C++ language (Borland Software Corporation, California, United States). All SECM experiments were carried out with a 25 μ m diameter Pt ultramicroelectrode (UME) fabricated according to Ref. [33] with $RG \approx 10$ ($RG = r_{\text{glass}}/r_T$), where r_{glass} is the radius of the UME insulating sheath and r_T is the radius of the active electrode. All electrochemical studies used a Pt-wire counter electrode and an Ag/AgCl/3 M KCl reference electrode to which all potentials are referred to. The in-house software MIRA was used to process and analyze the data [34].

The approach curves were recorded with three different redox mediators: [IrCl₆]^{3-/2-}, FcMeOH/Fc⁺MeOH and [Ru(NH₃)₆]^{3+/2+}. The redox mediator concentrations were 1 mM in aqueous 0.1 M KCl supporting electrolyte. All approach curves were carried out at scan rate $v = 1$ mm s⁻¹ and step size of 0.5 μ m. Prior to SECM experiment all SiO_x samples were rinsed with ethanol, distilled water and dried under a stream of Ar.

The potentials applied to the UME and SiO_x thin film were determined by cyclic voltammogram of the redox mediator on the UME and are given in Table 1.

2.3.3. AFM measurements

The samples were imaged with a Dimension 3100 model AFM (Veeco, Santa Barbara, CA) equipped with a Nanoscope IV controller (Digital Instruments) under ambient conditions. Single beam silicon cantilevers (AFM-TM Arrow, Nanoworld) with spring constants of ~ 42 N m⁻¹ and resonant frequencies of ~ 250 kHz were used. All AFM images were acquired in tapping mode at a constant force of 5–50 pN.

3. Results and discussion

3.1. Deposition of SiO_x thin films on gold

Silica films of three different thicknesses ranging between 7 and 40 nm were deposited on gold thin films using PECVD tech-

Table 1

Calculated effective rate constants (k_{eff}) from SECM approach curves on 6.6, 19.5 and 40.2 nm SiO₂ layers for [IrCl₆]³⁻ ($D_{\text{IrCl}_6} = 1.0 \times 10^{-5} \text{ cm}^2 \text{ s}^{-1}$), [Ru(NH₃)₆]³⁺ ($D_{\text{Ru}(\text{NH}_3)_6} = 7.4 \times 10^{-6} \text{ cm}^2 \text{ s}^{-1}$), and FcMeOH ($D_{\text{FcMeOH}} = 6.0 \times 10^{-6} \text{ cm}^2 \text{ s}^{-1}$)

ET (V)	E_s (V)	$k_{\text{eff}} (\times 10^{-4} \text{ cm s}^{-1})$		
		6.6 nm	19.5 nm	40.2 nm
[IrCl ₆] ³⁻	OCP	3.8 ± 0.76	3.57 ± 0.73	0.01 ± 0
	0.6	3.42 ± 0.68	3.26 ± 0.67	0.01 ± 0
	0.5	4.22 ± 0.84	2.38 ± 0.49	0.01 ± 0
	0.4	5.11 ± 1.02	3.00 ± 0.61	0.01 ± 0
[Ru(NH ₃) ₆] ³⁺	OCP	3.00 ± 0.33	3.11 ± 0.36	0.75 ± 0.08
	-0.1	3.37 ± 0.37	1.43 ± 0.17	0.85 ± 0.09
	0	3.51 ± 0.38	2.55 ± 2.93	0.73 ± 0.08
	0.1	3.85 ± 0.42	2.55 ± 0.29	0.73 ± 0.08
FcMeOH	OCP	6.20 ± 1.08	2.37 ± 0.41	0.17 ± 0.03
	0.1	6.94 ± 1.21	2.64 ± 0.29	0.01 ± 0
	0	6.59 ± 1.14	2.77 ± 0.67	0 ± 0
	-0.1	6.72 ± 1.17	2.66 ± 0.64	0.08 ± 0.01

nique. As discussed in our earlier papers [19–21], the process is based on the chemical vapor decomposition of a gas mixture of SiH₄ and N₂O in a plasma reactor at 300 °C. The thickness of the silica layer on gold was evaluated using ellipsometry and found to be: 6.6 ± 0.5 nm, 19.5 ± 0.5 nm and 40.2 ± 0.5 nm. The results were corroborated using surface plasmon resonance in the scanning mode where the variation of the reflected light as a function of the angle of incidence is monitored. The critical angle under which the light beam hits the interface and thus the angle of resonance Θ are characteristic for the system under study and any change in the refractive index or the thickness of the dielectric medium will cause the resonance angle to shift. Fig. 1 shows the shift in the resonance angle after SiO_x films of three different thicknesses have been deposited *ex situ* on the gold covered glass slide. While the critical angle is not shifting during the experiment as water was used as the solvent in all experiments, the angle where the surface plasmon resonance occurs is shifted to higher angles with increasing SiO_x thickness. The determination of the SiO_x layer thick-

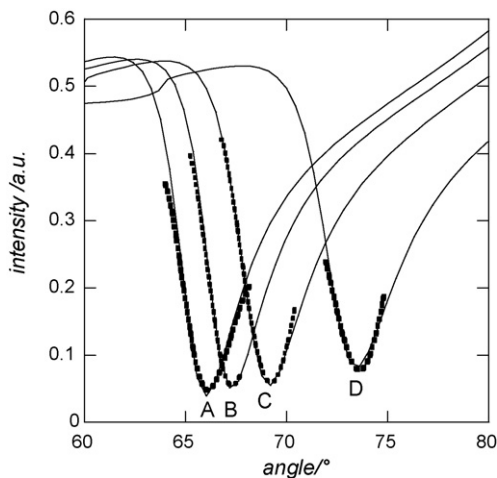


Fig. 1. Reflected light intensity versus incident angle curves for different thicknesses of deposited SiO_x on 50 nm thick gold layers on glass with a 5 nm titanium adhering layer. Dashed lines are experimental results; full lines are fitted curves: 0 nm (A), 6.6 nm (B), 19.5 nm (C) and 40.2 nm (D); fitting parameters: $n_{\text{(prism)}} = 1.58$, $n_{\text{(Au)}} = 0.197 + i3.442$ with $d = 53$ nm, $n_{\text{(Ti)}} = 2.36 + i3.112$ with $d = 5$ nm, $n_{\text{(SiO}_x)} = 1.48$ (fitting program: Winspall 2.01).

ness was achieved by fitting theoretical SPR working curves and the corresponding thicknesses were determined using the following parameters: $n_{\text{(prism)}} = 1.58$, $n_{\text{(Au)}} = 0.197 + i3.442$ with $d = 53$ nm, $n_{\text{(Ti)}} = 2.36 + i3.112$ with $d = 5$ nm, $n_{\text{(SiO}_2)} = 1.48$. The obtained thicknesses of SiO₂ are in good agreement with the expected values according to our experimental conditions and are comparable to those obtained from ellipsometric measurements. Gold–silicon dioxide interfaces with a SiO_x thickness higher than 60 nm did not show any SPR minimum on the glass prism used ($n = 1.58$) using the Autolab-ESPRIT.

3.2. Characterization of the gold/SiO_x films

3.2.1. Atomic force microscopy

The morphology of the gold interface before and after silica coating was investigated using AFM. Fig. 2A displays the tapping mode AFM image of a cleaned gold surface. The gold substrate displays a surface roughness of 0.546 RMS on an area of 1 μm^2 . Deposition of silica films on the surface did not induce any topographical changes of the surface. AFM images of the surfaces covered with 6–40 nm thick SiO_x films (Fig. 2B–D) exhibit similar features with increasing surface roughness (6.6 nm; RMS = 0.956, 19.5 nm; RMS = 1.155, 40.2 nm; RMS = 1.68; area of 1 μm^2). With the limit of the AFM resolution, no defects or pinholes were observed. After leaving the interfaces in water for 2 h, there was no evidence for morphology changes in the AFM images. This is characteristic of a free-pinhole surface.

3.2.2. Cyclic voltammetry measurements

Cyclic voltammetry (CV) of an electroactive redox couple is a valuable tool for testing the kinetic barrier properties of surface-modified electrodes. Fig. 3 compares the voltammetric responses obtained prior to the SiO_x film deposition and after PECVD deposition of SiO_x layers with different thicknesses. Fe(CN)₆⁴⁻ is oxidized as expected on the thin film electrode in a one electron process. A higher peak separation ($\Delta E_p = 130$ mV) compared to a massive gold electrode ($\Delta E_p = 60$ mV) is observed, due to higher resistivity of the thin gold film. For the SiO_x films with a thickness of 19.5 and 40.2 nm the behavior is characteristic for highly efficient barriers for the redox probe. The voltammetric signal as well as the current detected is largely suppressed. This blocking effect was maintained by leaving the interface for more than 4 h in an aqueous solution containing the redox mediator, in agreement with the existence of a highly dense oxide film, preventing the degradation of the hydrophilic SiO_x thin layer with time.

The capacitive current of 6.6 nm of SiO_x is less intense than those recorded on bare electrodes. This behavior is characteristic for barriers with a higher concentration of defect sites. The shape of the i - E signal remains, however, sigmoidal suggesting at the first look that the interface can be considered as an assembly of ultramicroelectrodes, where the presence of bare gold spots are exposed to the solution. Fig. 3 (curve 2) suggests, at the first look, that the 6.6 nm SiO_x layer on Au behaves like an array of microelectrodes. It is important to remember however that it does not necessarily indicate the presence of bare Au spots (“true” pinholes) exposed to the solution. In view of the SECM data (no active spots visible in the scan, see 3.2.3.) it rather indicates that those “pinholes” are blocked by a layer of SiO_x that is thin enough to allow diffusively controlled current under experimental timescale used. One obvious test to prove/disprove this hypothesis is to investigate the scan rate dependence of the CV curves such as the curve 2 from Fig. 3. If E1/2 is scan rate independent, then we have a very small areas of Au exposed to the solution. If E1/2 shifts towards negative potentials with increasing scan rate than we can easily imagine having

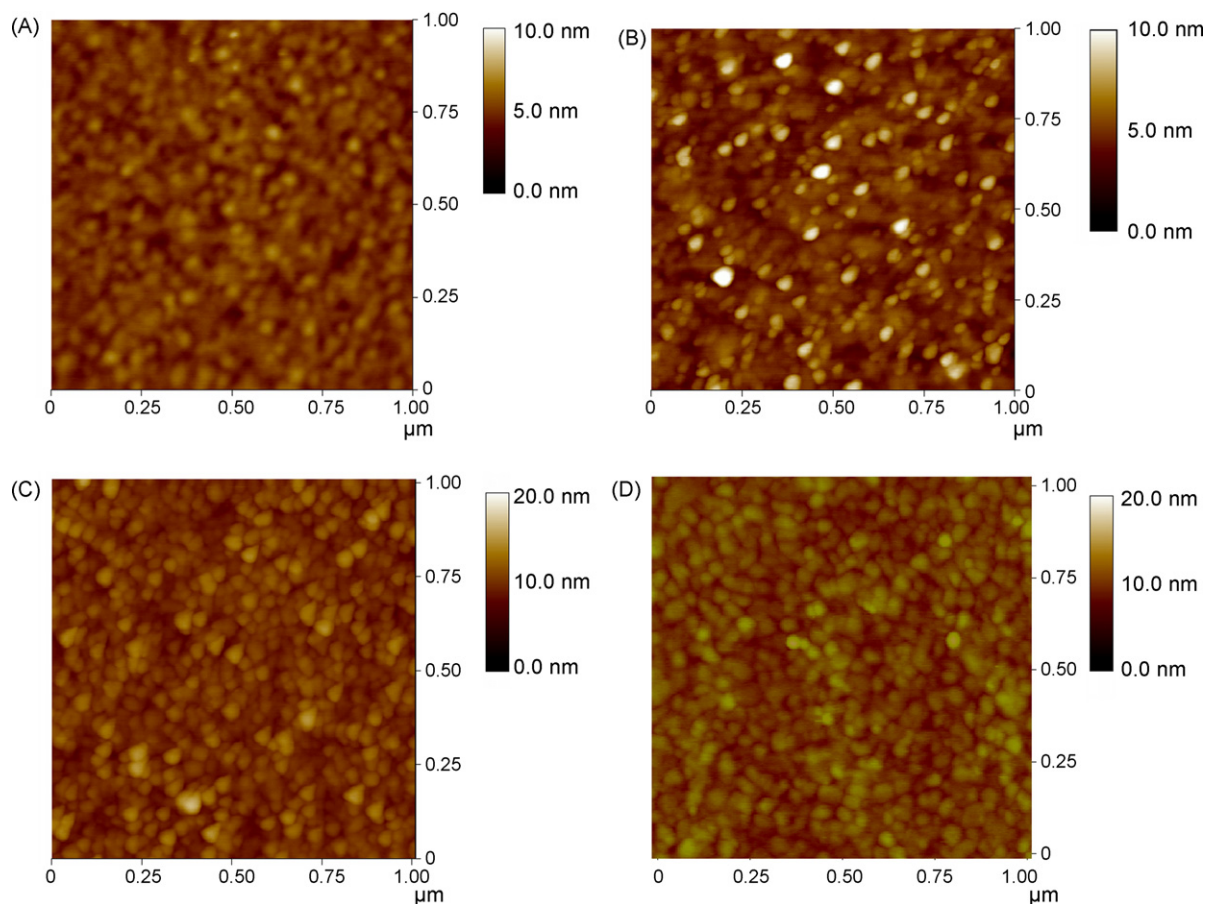


Fig. 2. Tapping mode AFM images of the gold surface before (A) and after coating with 6.6 nm (B), 19.5 nm (C) and 40.2 nm (D) thick SiO_x layer.

20 μm or larger defects containing fairly thin layer of blocking SiO_x , allowing tunneling of electrons between solution species and Au. $E_{1/2}$ proved to be scan rate independent and the presence of small pinholes exposing gold to the solution is the more probable situation.

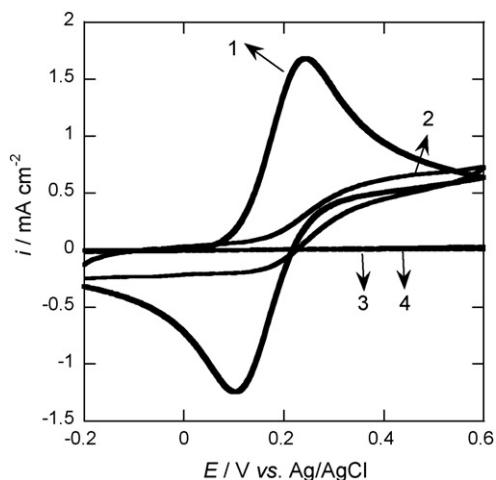


Fig. 3. Cyclic voltammetry curves for a 50 nm thick polycrystalline gold film on glass with 5 nm titanium adhesion layer (1) and the same electrode covered with 6.6 nm SiO_x (2), 19.5 nm SiO_x (3), 40.2 nm SiO_x (4); solution: 10 mM $\text{Fe}(\text{CN})_6^{4-}$ in KCl (0.1 M/water), scan rate: 0.05 V s^{-1} . Curves 3 and 4 overlap.

3.2.3. Scanning electrochemical measurements

SECM images showed no resolvable pinholes in agreement with the absence of detectable pinholes in the AFM images with a resolution better than 10 nm. Therefore SECM approach curves were used to detect the presence of very small pinholes by their influence on the substrate kinetics. Three redox mediators with different charges were used in order to make the approach curves: $[\text{Ru}(\text{NH}_3)_6]^{3+}$, $[\text{IrCl}_6]^{3-}$ and FcMeOH.

The SECM approach curve records the UME current i_T as a function of the vertical position z of the UME. The UME generates high local concentration of one form of a redox mediator, e.g. the reduced form R over the sample. The diffusion-limited current recorded at the UME depends on the regeneration rate of R at the sample. When the sample is biased at a potential where the recycling of the mediator is slow, the sample acts as an insulator and the current at the UME decreases (negative feedback). However, when the potential of the sample is poised to a sufficient negative potential where the mediator R is re-oxidized to O at a diffusion-controlled rate, the sample acts as a conductor and the UME current increases. Between these potentials, the UME current depends on the rate of electron-transfer ET at the sample and rate of diffusion of the regenerated mediator to the UME [35]. Different overpotentials were applied to the sample in order to monitor changes at the rate of the electron transfer. The potential range was selected according to the formal potentials of each mediator.

A normalized rate constant κ is obtained from the fit of the experimental approach curve to theory [36,37]. Knowing r_T and the diffusion coefficient of the mediator D once can calculate

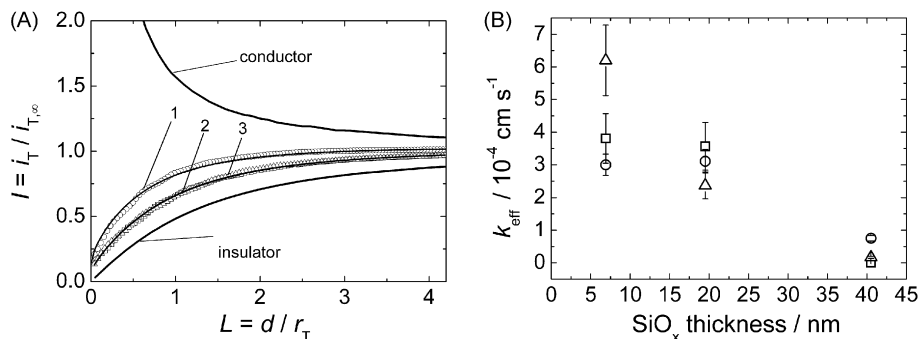


Fig. 4. (A) Normalized approach curves towards 6.6 nm SiO_x deposited on gold using different redox mediators: (1) $\text{FcMeOH}/\text{Fc}^+\text{MeOH}$, (2) $[\text{Ru}(\text{NH}_3)_6]^{3+/2+}$, (3) $[\text{IrCl}_6]^{3-/2-}$. The applied UME potentials were $E_T = 0.4$, -0.4 and 0.9 V respectively and the sample was left at OCP. The corresponding κ values extracted from the curve fitting were: (1) 0.136, (2) 0.050 and (3) 0.049. The open symbols correspond to experimental curves and the lines to theoretical fittings. The thick lines represent the theoretical approach curves for an UME over a conductive and an insulating substrate from Ref. [36]. (B) Dependence of k_{eff} on SiO_x layer thickness. (\square) $[\text{IrCl}_6]^{3-}$, (\circ) $[\text{Ru}(\text{NH}_3)_6]^{3+}$ and (Δ) FcMeOH . $E_s = \text{OCP}$.

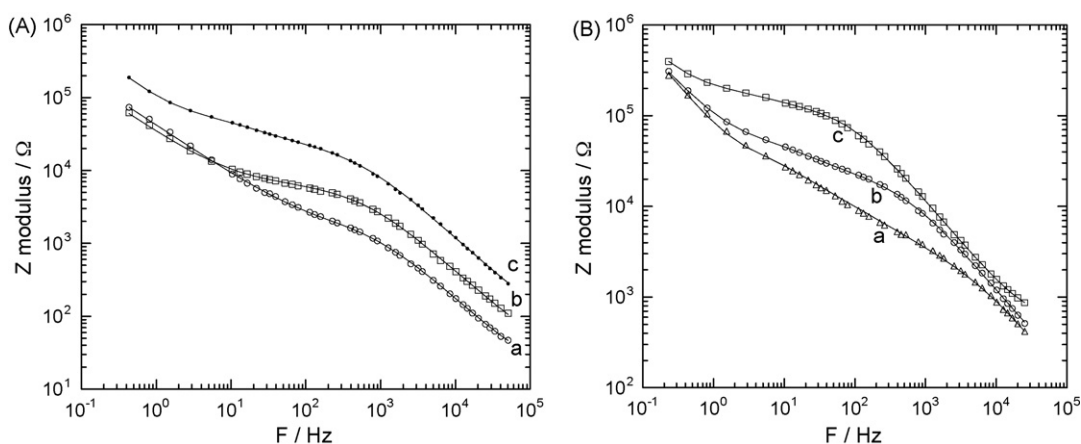


Fig. 5. Bode plot for (A) gold/ SiO_x interfaces (a) 6.6 nm, (b) 19.5 nm, (c) 40.2 nm in 0.1 M KCl/water and (B) on gold/ SiO_x (40.5 nm) in (a) 1 M KCl/water, (b) 0.1 M KCl/water and (c) 0.01 M KCl/water; experimental data (symbols), fitted data (line), the measured frequency range is 100 kHz to 1 Hz with a 10 mV RMS signal applied under open circuit conditions.

k_{eff} :

$$k_{\text{eff}} = \kappa \cdot \frac{D}{r_T} \quad (1)$$

Fig. 4A shows the normalized approach curves on gold/ SiO_x (6.6 nm) interface using three different redox mediators where the interface was not biased. The calculated k_{eff} for the three mediators were close to that of an insulator, $3.8 \times 10^{-4} \text{ cm s}^{-1}$, $3.0 \times 10^{-4} \text{ cm s}^{-1}$, $6.2 \times 10^{-4} \text{ cm s}^{-1}$ for $[\text{IrCl}_6]^{3-}$, $[\text{Ru}(\text{NH}_3)_6]^{3+}$ and FcMeOH , respectively. The positively and negatively charged mediators showed a lower rate of regeneration than the neutral mediator. However, as the thickness of the SiO_x increases this difference becomes negligible (Fig. 4B). The dependence of k_{eff} on the thickness of SiO_x is shown in Fig. 4B while the substrate was left at the open circuit potential (OCP). The rate of ET decreases with increasing layer thickness and for a SiO_x thickness of 40.2 nm approximately the same value is extracted for all the three different mediators.

Furthermore, the influence of the applied potential on the substrate on the rate of heterogeneous electron transfer was investigated. Negative feedback currents were observed in all three cases. The applied potentials to the SiO_x layers were not sufficiently negative (in the case of FcMeOH and $[\text{IrCl}_6]^{3-}$) or positive ($[\text{Ru}(\text{NH}_3)_6]^{3+}$) to influence the SiO_x electronic structure, thus the k_{eff} extracted from the curve fitting were rather constant. Table 1 is

summarizes the obtained rate constants of heterogeneous electron transfer using the different mediators with different applied potentials and different interfaces. The 6.6 nm SiO_x interfaces showed slightly faster ET than 19.5 and 40.2 nm thick interfaces indicating that it has more defect sites, and thus the mediator could diffuse through these sites and could be regenerated at the underlying gold substrate. Among the interfaces, the 40.2 nm SiO_x interfaces showed the best insulating feature providing k_{eff} values close to that of an insulating layer, even when an overpotential was applied.

3.2.4. Electrochemical impedance analysis

Electrochemical impedance analysis was performed on the gold/ SiO_x interfaces in aqueous solutions containing different concentrations of KCl as supporting electrolyte. Fig. 5 shows the evolution of the impedance behavior of the interfaces with increasing SiO_x thickness (Fig. 5A) and at different electrolyte con-

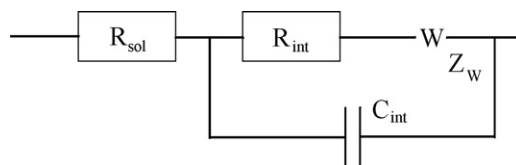


Fig. 6. Scheme of used equivalent circuit.

Table 2Values of equivalent circuit elements obtained by fitting the experimental data for gold/SiO_x interfaces 6.6, 19.5 and 40.2 nm in 0.1 M KCl/water

Interface	R_{int} (Ω)	C_{int} ($\times 10^{-8}$ F)	F_{int} (Hz)	n_{int}	$W-R$ (Ω)	$W-T$ (s)	$W-P$
6.6 nm	775 \pm 24	9.8 \pm 0.3	2106	0.943	3130 \pm 90	0.003	0.34
19.5 nm	4070 \pm 130	4.87 \pm 0.15	804	0.903	6950 \pm 200	0.018	0.35
40.2 nm	14200 \pm 400	1.64 \pm 0.05	685	0.923	101000 \pm 3000	0.197	0.41

Table 3Values of equivalent circuit elements obtained by fitting the experimental data for gold/SiO_x (40.2 nm) in aqueous 1 M, 0.1 M and 0.01 M KCl

Solution	R_{int} (Ω)	C_{int} ($\times 10^{-8}$ F)	F_{int} (Hz)	n_{int}	$W-R$ (Ω)	$W-T$ (s)	$W-P$
1 M KCl	1360 \pm 40	1.45 \pm 0.05	8048	0.974	88500 \pm 2700	0.193	0.46
0.1 M KCl	14200 \pm 400	1.64 \pm 0.05	685	0.923	101000 \pm 3000	0.197	0.41
0.01 M KCl	98000 \pm 3000	1.66 \pm 0.05	98	0.917	154000 \pm 4600	0.245	0.37

concentrations keeping the thickness of SiO_x constant (Fig. 5B). An equivalent circuit was designed in order to fit the impedance spectra obtained (Fig. 6). For the high frequency domain, the circuit includes the ohmic resistance of the electrolyte solution; for intermediary and low frequency domains, a resistance R_{int} in series with a finite length Warburg impedance and in parallel with interface capacitance C_{int} were used. The resistance R_{int} was globally attributed to the Au/SiO_x interface, the SiO_x layer and the SiO_x/electrolyte interface. In a first approximation, the capacity C_{int} was also attributed to these three parts of the interface. The lines in Fig. 5 correspond to the fit using the equivalent circuit model.

Table 2 shows values of the circuit elements obtained by fitting of the experimental data. The capacitance C_{int} obtained is in the order to 10⁻⁸ F, which is too low to be attributed to a solid/solution interface. Moreover, it was observed that C_{int} is independent of the electrolyte concentration. It can be thus concluded that C_{int} is principally governed by the thickness of the layer of SiO_x. Similar results have been shown for SiO₂ layers on silicon [38,39]. In addition, the thickness of thin oxide layers has been determined by impedance spectroscopy with the calculation of capacitance [40].

The resistance R_{int} changes with the SiO_x thickness and with the electrolyte concentration. This resistance is thus indeed the sum of three resistors in series related to the Au/SiO_x interface, the SiO_x layer and the SiO_x/electrolyte interface. The parameters related to the Warburg impedance are given in the last three columns in Table 2. The resistance $W-R$ associated with the particle diffusion is large when the SiO_x layer is thick or when the electrolyte concentration is low. The time constant $W-T$ is also related to the thickness of SiO_x. However, it is independent of the concentration of the solution (Table 3). As $W-T = \delta^2/D$ with δ being the diffusion layer thickness and D the diffusion coefficient, this suggests that the diffusion layer thickness is related to the thickness of the SiO_x layer. The SiO_x layer acts as a diffusion barrier. These results confirm those obtained by cyclic voltammetry and SECM.

4. Conclusion

The electrochemical behavior of thin gold film electrodes coated with silicon dioxide layers of different thickness was investigated using cyclic voltammetry, SECM and EIS. SECM images showed no resolvable pinholes in agreement with the absence of detectable pinholes using AFM. However, SECM approach curves allowed determining the presence of very small pinholes by recording changes in the heterogeneous rate constant of different redox mediators to the gold/SiO_x interfaces. The 6.6 nm thick SiO_x interface showed slightly faster electron transfer, while an insulating behavior was observed on the 40.2 nm SiO_x interface. EIS and cyclic

voltammetry measurements confirmed the barrier effect of the SiO_x layer. It was in particular observed that the interface capacitance is governed by the thickness of the oxide layer.

Acknowledgments

The Agence Nationale de la Recherche (ANR), the Centre National de la Recherche Scientifique (CNRS), the Institut National Polytechnique de Grenoble (INPG) and the Nord-Pas-de Calais region are gratefully acknowledged for financial support. S. Szunerits thanks the Hanse Wissenschaftskolleg for a 3.5 months fellowship. The project was partially supported by DFG Wi 161718.

References

- [1] M. Etienne, A. Walcarius, *Electrochem. Commun.* 7 (2005) 1449.
- [2] O. Lev, Z. Wu, S. Bharathi, V. Glezer, A. Modestov, J. Gun, L. Rabinovich, S. Sampath, *Chem. Mater.* 9 (1997) 2354.
- [3] M. Tsionsky, G. Gun, V. Glezer, O. Lev, *Anal. Chem.* 66 (1994) 1747.
- [4] M. Tsionsky, O. Lev, *Anal. Chem.* 67 (1995) 2409.
- [5] A. Walcarius, *Chem. Mater.* 13 (2001) 3351.
- [6] J. Wang, P.V.A. Pamidi, D.S. Park, *Anal. Chem.* 68 (1996) 2705.
- [7] T. Yamane, N. Nagai, S.-I. Katayama, M. Todoki, *J. Appl. Phys.* 91 (2002) 9772.
- [8] N. Ariel, G. Ceder, D.R. Sadoway, E.A. Fitzgerald, *J. Appl. Phys.* 98 (2005), 023516/1.
- [9] D.K. Kambhampati, T.A.M. Jakob, J.W. Robertson, M. Cai, J.E. Pemberton, W. Knoll, *Langmuir* 17 (2001) 1169.
- [10] H.B. Liao, W. Wen, G.K.L. Wong, *J. Appl. Phys.* 93 (2003) 4485.
- [11] S. Bharathi, M. Nogami, S. Ikeda, *Langmuir* 17 (2001) 1.
- [12] M. Opallo, J. Kukulka, *Electrochem. Commun.* 2 (2000) 394.
- [13] S. Sayen, A. Walcarius, *Electrochem. Commun.* 5 (2003) 394.
- [14] A. Walcarius, D. Mandler, J.A. Cox, M. Collinson, O. Lev, *J. Mater. Chem.* 15 (2005) 3663.
- [15] A. Graneli, J. Rystrom, B. Kasemo, F. Hook, *Biosens. Bioelectron.* 20 (2004) 498.
- [16] K. Glasmar, C. Larsson, F. Hook, B. Kasemo, *J. Colloid Interface Sci.* 246 (2002) 40.
- [17] C. Larsson, M. Rodahl, F. Hook, *Anal. Chem.* 75 (2004) 5080.
- [18] E. Reimhult, C. Larsson, B. Kasemo, F. Hook, *Anal. Chem.* 76 (2004) 7211.
- [19] S. Szunerits, R. Boukherroub, *Langmuir* 22 (2006) 1660.
- [20] S. Szunerits, Y. Coffinier, S. Janel, R. Boukherroub, *Langmuir* 22 (2006) 10716.
- [21] S. Szunerits, R. Boukherroub, *Electrochem. Commun.* 8 (2006) 439.
- [22] I. Zawica, G. Wittstock, R. Boukherroub, S. Szunerits, *Langmuir* 23 (2008) 9303.
- [23] I. Zawica, G. Wittstock, R. Boukherroub, S. Szunerits, *Langmuir* 24 (2008) 3922.
- [24] S. Szunerits, S.E. Pust, G. Wittstock, *Anal. Bioanal. Chem.* 74 (2007) 3122.
- [25] M.E. Williams, K.J. Stevenson, A.M. Massari, J.T. Hupp, *Anal. Chem.* 72 (2000) 3122.
- [26] T. Ito, A.A. Audi, G.P. Dible, *Anal. Chem.* 78 (2006) 7048.
- [27] C. Nunes Kirchner, K.H. Hallmeier, R. Szargan, T. Raschke, C. Radehaus, G. Wittstock, *Electroanalysis* 19 (2007) 1023.
- [28] S.E. Pust, D. Scharnweber, S. Baunack, G. Wittstock, *J. Electrochem. Soc.* 154 (2007) C508.
- [29] S.E. Pust, D. Scharnweber, C. Nunes Kirchner, G. Wittstock, *Adv. Mater.* 19 (2007) 878.
- [30] A.K. Neufeld, A.P. O'Mullane, *J. Solid State Electrochem.* 10 (2006) 808.
- [31] T. Wink, S.J. Van Zuilen, A. Bult, W.P. van Bennekom, *Anal. Chem.* 70 (1998) 827.
- [32] R.P.H. Kooyman, A.T.M. Lenferink, R.G. Eenik, J. Greve, *Anal. Chem.* 63 (1991) 83.
- [33] C. Kranz, M. Ludwig, H.E. Gaub, W. Schuhmann, *Adv. Mater.* 7 (1995) 38.

- [34] G. Wittstock, T. Asmus, T. Wilhelm, *Fresenius J. Anal. Chem.* 367 (2000) 346.
- [35] B.R. Horrocks, M.V. Mirkin, A.J. Bard, *J. Phys. Chem.* 98 (1994) 9106.
- [36] R. Cornut, C. Lefrou, *J. Electroanal. Chem.* (2008), doi:10.1016/j.jelechem.2007.09.021.
- [37] J.L. Amphlett, G. Denuault, *J. Phys. Chem. B* 102 (1998) 9946.
- [38] P. Schmuki, H. Böhni, J.A. Bardwell, *J. Electrochem. Soc.* 142 (1995) 1705.
- [39] O. Purrucker, H. Hillebrandt, K. Adlkofer, M. Tanaka, *Electrochim. Acta* 47 (2001) 791.
- [40] M. Chemla, V. Bertagna, R. Erre, F. Rouelle, S. Petitdidier, D. Levy, *Appl. Surf. Sci.* 227 (2004) 193.